ASSESSING INTERLAMINAR SHEAR STRESS-STRAIN CURVES IN TAPE COMPOSITES BASED ON THE FLAT-PLATE TORSION METHOD

by

GARY STEVEN GROHMAN JR

Presented to the Faculty of the Graduate School of

The University of Texas at Arlington in Partial Fulfillment

of the Requirements

for the Degree of

MASTER OF SCIENCE IN AEROSPACE ENGINEERING

THE UNIVERSITY OF TEXAS AT ARLINGTON

MAY 2015

Acknowledgements

I would like to take this time to thank The University of Texas Arlington for providing me the ability to do research and making this thesis possible. I would like to thank the Testing and R&D Center at Triumph Aerostructures – Vought Aircraft Division for providing material, equipment, and funding for this research.

I would also like to think my thesis committee chairman Dr. Andrew Makeev and my committee members Dr. Ashfaq Adnan and Dr. Yuri Nikishkov. Without the support from this committee my research would not have been possible. A special thanks is for Debi Barton, the Graduate Mechanical and Aerospace departmental support for all her help in guiding me through the program with such a positive and cheerful attitude.

My colleagues, Dr. Guilluame Seon, Julia Cline, and Bastiaan Van Der Vossen provided me invaluable knowledge and moral support that allowed me to keep moving forward even when things did not go as planned. Special thanks is for Brian Shonkwiler for his help in creating test fixtures, preparing specimen, running tests, and working to the fast paced schedule research often demands.

I would like to thank my fiancée Megan Criswell for the day to day moral support to keep going when I lost the motivation to do so. I would like to thank her for supporting me through this tough time even though it meant many days, months, and years of little or no time to spend together. I would also like to thank my parents for their support to pursue an education. I would especially like to thank my grandmother because without your support and encouragement I would never have made it into the aerospace industry and been able to achieve this.

May 16, 2015

Abstract

ASSESSING INTERLAMINAR SHEAR STRESS-STRAIN CURVES IN TAPE COMPOSITES BASED ON THE FLAT-PLATE TORSION METHOD

Gary Steven Grohman Jr. M.S.

The University of Texas at Arlington, 2015

Supervising Professor: Andrew Makeev

Composites are attractive for structural applications in the aerospace industry for their high strength to weight ratio, stiffness, and low density. The development and implementation of composite structures has grown rapidly through the aerospace industry exceeding our ability to characterize the material properties due to costly and time consuming test methods. The ability to fully characterize the nonlinear stress-strain relationship in the 1-3 and 2-3 principal planes up to the point of failure is extremely important for predicting failures in composites. The principal directions for composites are the fiber direction, transverse direction, and the thru thickness direction, commonly referred to as the 1, 2, 3 directions.

Conventional testing such as short beam shear (SBS) and V-notch tests are used in industry to determine the interlaminar shear properties of composites. With the use of the digital image correlation (DIC) technique and finite element analysis (FEA), SBS tests have been developed to include the measurement of multiple material constitutive properties, including nonlinear interlaminar shear stress-strain curves in the 1-3 principal material plane. However, SBS and V-notch testing are limited to measuring linear interlaminar shear material properties in the 2-3 direction, due to premature tensile failure due to bending before the stress-strain relation becomes nonlinear.

By loading a flat plate composite specimen in compression with the contact surfaces on the corners of the opposite upper and lower surface to create a torsional deformation, significant nonlinear shear strain is developed on all principal material planes. Using DIC, the nonlinear interlaminar shear strain can be obtained in the 2-3 direction experimentally. Multiple test methods were conducted to assess the effects of different configurations to eliminate the sensitivity of the placement of the loading surfaces and by varying the length, width, and thickness of the specimen and the diameters and shapes of the loading nodes.

Measured material properties from SBS tests were used as an initial approximation in an iterative FEA implemented using Abaqus. The FEM based stresses calculated in the flat plate torsion specimens were used to establish the interlaminar shear stress-strain curves based on the surface strain components measured using DIC. Strain data was simultaneously captured on the 1-3 and 2-3 planes. Analysis of the 1-3 plane using the flat plate torsion method was verified with SBS testing. Analysis in the 2-3 planes was verified in the linear region of SBS and provides an indication that the FPT test method can accurately measure nonlinear interlaminar shear in the 2-3 plane.

Table of Contents

List of Illustrations

List of Tables

Chapter 1

Introduction

Composites are attractive for structural applications in the aerospace industry for their high strength to weight ratio, stiffness, and low density. The development and implementation of composite structures and the ability to understand the material properties to aid in design and analysis promote the advancement of composites in industry. The rate of growth of implementing composites structures has vastly surpassed the ability to understand material characterization. This is because material characterization testing is time consuming and very expensive. Therefore more conservative estimates are being used in place of actual measurements. In order to completely understand failure mechanisms of composites under complex loading three dimensional material properties are necessary. Conservative in plane properties are being used as assumptions to describe the out of plane properties causing over design of structures increasing weight and cost. Northrop Grumman's RQ-4 Global Hawk is an example of leading edge composite technology. The wing of this autonomous high altitude, high aspect ratio, surveillance plane is purely high strength low weight scaled composites.

The ability to do more predictions using FEA methods significantly reduces the cost to test and design new structures. To fully understand complex deformation and failure mechanisms in composite structures, three dimensional material properties in all principal directions are required. The principal directions for composites are the fiber direction, transverse direction, and the thru thickness direction, commonly referred to as the 1, 2, 3 directions. Figure 1-1 shows a typical orientation of the principal directions of a carbon coupon specimen identified in 1-2-3 direction.

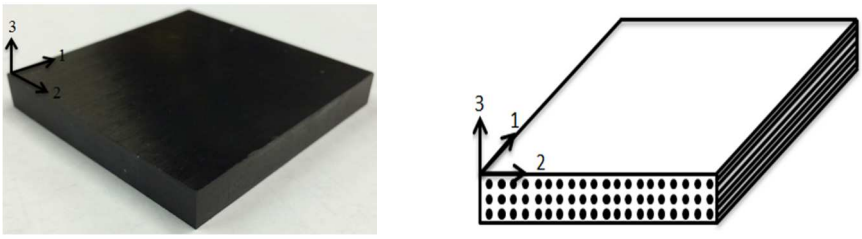

Figure 1-1 Principal directions of a carbon specimen

Tensile, compressive, and shear material constitutive properties are used to analyze composites. In-plane and out-of-plane properties are distinguished in composites due to the anisotropic behavior between the matrix and fibers having different directional material properties. Non-linear shear stress-strain behavior is typically observed in polymer matrix composite materials. Current test methods such as short beam shear (SBS) and V-notch testing exist to produce shear strength properties and interlaminar properties. SBS shear and V-notch testing are limited to measuring linear shear material properties in the 2-3 direction, due to premature tensile failure due to bending before the stress-strain curve becomes nonlinear. The failure modes of SBS are generally compressive failure due to the contact surfaces, tensile failure due to bending, and shear failure. Figure 1-2 illustrates the failure modes of SBS specimen.

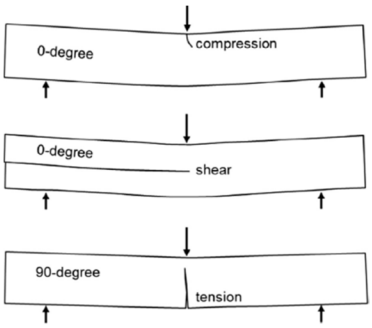

Figure 1-2 Short beam shear failure modes

During testing the specimen undergoes bending and puts the upper surface in compression and the lower surface in tension. In the 1-3 plane the fiber strength is

strong and withstands the transverse strain forcing the specimen to fail in shear due to delamination of the plies instead of tension. In the 90-degree direction, or the 2-3 plane the strength of the matrix is weaker and not able to resist the transverse strain causing the specimen to fail in tension. Figure 1-3 illustrates the deformation of a SBS specimen.

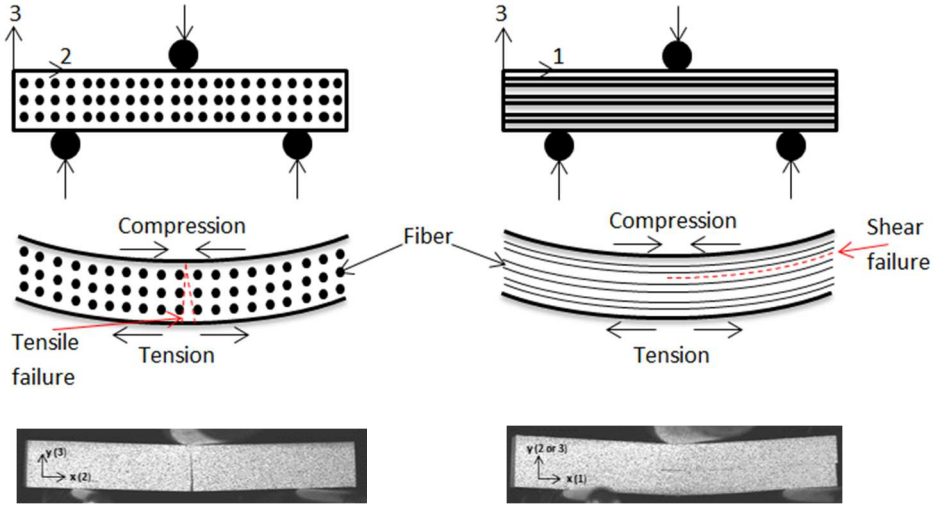

Figure 1-3 Deformation of a SBS specimen under load

The most common test method to determine the interlaminar shear strength of composites is by a short beam shear test (ASTM D2344M-00). It has been shown that SBS specimen are geometrically material independent allowing for closed loop form calculations of stress using experimentally determined strains. In structural design stress-strain curves are used to determine numerous material properties such as the modulus of elasticity, shear modulus, and yield strength. Interlaminar shear material properties are difficult to characterize using conventional test methods such as SBS. In the pursuit of methods for measuring multiple mechanical properties in carbon tape composites simultaneously, the flat plate torsion test method is considered for assessment of interlaminar shear stress-strain curves in 2-3 principal plane.

Flat plate torsion tests have been used for decades to asses in plane material properties of composites. Tsai proposed a method using pure twisting of unidirectional plates to determine elastic properties. (1) Howell tested a flat plate specimen in an attempt to determine the critical dimensionless twist, κα using 2 strain gage rosettes. (2) He found that there is a linear relationship between κα at bifurcation and the thickness to edge length ratio, h/a. (2) Loading a flat plate carbon specimen as shown in Figure 1-4 produces a torsional reaction along the principal directions. (2) In 1996 a paper was published on the effects of point loading indentation into the specimen. The authors attempted to measure the in-plane shear modulus using a flat plate torsion specimen. (3) They indicated the use of cylindrical rollers eliminated indentation during testing of the specimen as seen in Figure 1-4 .

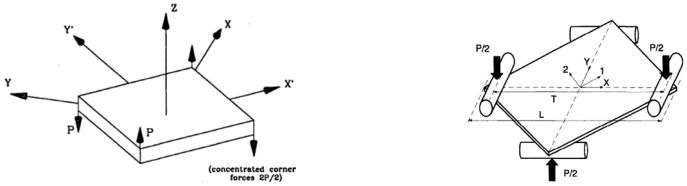

Figure 1-4 Torsional loading of a flat plate carbon specimen (2) (left) and modified flat plate test specimen (3) (right)

In 2013 an article published by Elsevier in Composites: Part A, load-displacement curves were used to measure the in-plane shear stress-strain relationship using the flat plate torsion test method. (4) The article concludes that the lower failure stresses were experienced possibly due to surface defects or spurious transverse tensile stresses. (4) However, calculated shear-stress strain curves were consistent with the results of tensile tests conducted on angle-ply coupons and that unidirectional plate torsion testing was worth considering further research. (4)

With the intention to develop three-dimensional properties in all principal directions simultaneously, Dr. Andrew Makeev, the Director of the Advanced Materials and Structures Lab at the University of Texas Arlington, began testing flat plate torsion specimen in September of 2013. A paper recently published in June of 2014 in Composites Science and Technology showed the ability to measure multiple principal planes during one test simultaneously. A 2.5" square flat plate torsion specimen 0.25" thick was used with 0.375" spherical contact surfaces. The interlaminar shear curves were consistent with SBS curves and the 2-3 plane strains reached 3%. (5) SBS test typically fail near 1% strain in the 2-3 plane before the curves becomes nonlinear. The ability to get the strains to 3% allowed for the nonlinear shear stress-strain relationship in the 2-3 principal plane to be shown.

The effects of stress concentrations due to contact from loading are assessed in this research by varying the diameter and shape of the contact surfaces. SBS tests have been developed to eliminate compressive failure due to the contact surfaces by varying the diameters of the contact surfaces which allow the specimen to have a shear failure mode. SBS tests have shown a relationship between the ratio of the support span and the thickness of the specimen. A support span to thickness ratio, s/t, illustrated in Figure 1-5, in the range of 4 to 8 has been shown to be sufficient for the specimen to fail in shear when paired with the proper diameter contact surfaces. Specimen geometry was varied in this research to determine the sensitivity of the specimen geometry to the FPT test method and to develop a test configuration that will provide a shear failure in the 2-3 plane. This will also provide more evidence for the assessment of material properties using this FPT method. Similar results from different test setups and configurations will

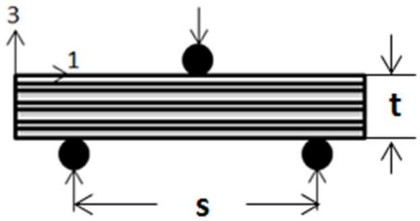

Figure 1-5 Support span and thickness ratio of a SBS specimen

provide some evidence the results from the testing are not specific to the test setup and can be applied over a number of different test setups. Analysis of the 1-3 plane using the flat plate torsion method is validated with SBS testing. Analysis of the 2-3 plane is validated in the linear regime of SBS tests and provides the nonlinear interlaminar shear stress-strain curve.

Chapter 2

Materials

Conventional monolithic materials can be broken up in to 3 main categories including metals, ceramics, and polymers. (6) Composites are a combination of 2 or more of these materials from any of the 3 categories. A basic composite specimen is broken up into 3 parts; a reinforcement, a matrix, and an interphase. (6) The reinforcement can be continuous or discontinuous, strong, and stiff while the matrix is generally weaker and continuous. Sometimes the chemical interaction between the reinforcement and the matrix will cause a distinct interphase to exist. (6) Properties of composite materials depend on a number of things including the geometry and matrix reinforcement interaction. One of the most important parameters of composites is the ratio or volume percent of the reinforcement also known as the fiber volume ratio. (6) Carbon composites generally have high stiffness and maintain good strength at high temperatures while having low density properties and low thermal expansion.

Carbon Composites

Because of its high strength to weight ratio, carbon composites are widely used in the aerospace, automotive, and sports industry. A carbon composite structure or fiber reinforced polymer (FRP) composite structure is made up of a fiber, matrix, and laminates. Varying the fiber direction during the layup process will allow for the composite structure to be designed to withstand different loading situations based on the loading the structure will see during application. The matrix is usually an epoxy which will bind the matrix and reinforcement together. Composite structures are designed to mostly carry longitudinal loads and therefore the fiber properties control the stiffness of the structure. However, out of plane deformation is controlled by the resin properties. Stress strain curves are often used to compare different materials strength and stiffness

properties. Also, the modulus of elasticity and shear modulus can be calculated from these curves. Using curves such as these, trends can be developed to classify different materials for different uses. In general as you increase the strength or stiffness you have a trade off in strain percent. This tends to make the material more brittle and will tend to fail suddenly without elongation or deformation. In some applications this is a favorable property.

IM7-8552 is a high performance continuous fiber reinforced carbon material for primary use in the aerospace industry. (7) The IM 7 fiber exhibits high tensile strength and modulus, good shear strength, and allows designers to maintain higher safety margins for both stiffness and strength. (8) Table 2-1 shows the physical properties of IM7-8552 and Table 2-2 shows the mechanical properties for IM7-8552. (8) IM7-8552 uses a prepreg thermoset resin which cures at elevated temperatures. (9) Prepreg resin is a roll of carbon fiber that has been saturated in a matrix. In this case as long as the carbon is kept at sufficient low temperatures the matrix will not begin to cure to the fiber. Parts can directly be laid up and then bagged and sent to the autoclave for curing.

Table 2-1 Physical properties of IM7-8552

	Units	IM7
Fiber Density	g/cm^3 (lb/in^3)	1.77 (0.064)
Filament count/tow		12k
Resin density	g/cm^3 (lb/in^3)	1.30 (0.047)
Nominal Cured Ply Thickness 8552/35%/134	mm (inch)	0.131 (0.0052)
Nominal Fiber Volume	%	57.70
Nominal Laminate Density	g/cm^3 (lb/in^3)	1.57 (0.057)

Table 2-2 Mechanical Properties of IM7-8552

Test	Units	Temp °C (°F)	Condition	IM7

Table 2-2 – Continued

0° Tensile Strength	MPa (ksi)	-55(-67)	Dry	2572
	MPa (ksi)	25(77)	Dry	(373)
		91(195)	Dry	2724 (395)
90° Tensile Strength		-55(-67)	Dry	**2538 (368)***
		25(77)	Dry	
		93(200)	Dry	174(25.3)
				164 (9.3)
				92 (13.3)*
0° Tensile Modulus	GPa (msi)	-55(-67)	Dry	163 (23.7)
	GPa (msi)	25(77)	Dry	164(23.8)
		91(195)	Dry	**163 (23.7)***
90° Tensile Modulus		-	-	-
		25(77)	Dry	
		93(200)	Dry	12(1.7)
				10(1.5)*
0° Compression Strength	Mpa (ksi)	-55(-67)	Dry	-
		25(77)	Dry	1690 (245)
		91(195)	Dry	1483 (215)
0° Compression Modulus	GPa (msi)	-55(-67)	Dry	-
		25(77)	Dry	150 (21.7)
		91(195)	Dry	162 (23.5)
0° ILSS (Shortbeam shear)	Mpa (ksi)	-55(-67)	Dry	-
		25(77)	Dry	137 (19.9)
		91(195)	Dry	**94 (13.6)***
		25(77)	Wet	115 (16.7)
		71(16)	Wet	**80 (11.6)****
		91(195)	Wet	-
In-plane shear strength	Mpa (ksi)	25(77)	Dry	120 (17.4)
		93(200)	Dry	**106 (15.4)***

Bold 93°C (200°F) **Bold* 104°C (220°F)** **Bold** 82°C (180°F)**

Specimen Layup and Curing

The specimen used for the flat plate torsion test were laid up and cured at Triumph Aerostructures – Vought Aircraft Division in Dallas, Texas. They were vacuum bagged and then processed in an autoclave. The procedure for laying up the specimen begins by cutting the material off the roll into the correct size. Typically 1" of excess around the border of the specimen is assumed as cutoff and will not be used in the actual parts. The cured per ply thickness of each ply is 0.0065". Typically every 5 plies were compacted in a compaction table individually as shown in Figure 2-1.

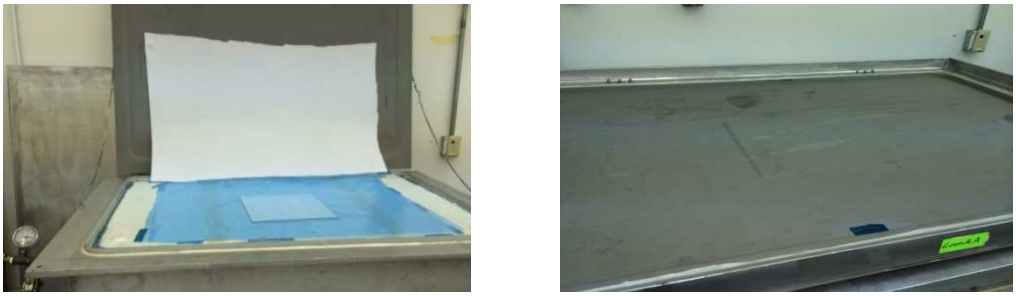

Figure 2-1 Compaction table

Once the specimens have been cut the bagging process is next. The bagging process is illustrated in Figure 2-3. There are numerous ways to bag parts depending on the fiber, matrix, and cure cycle.

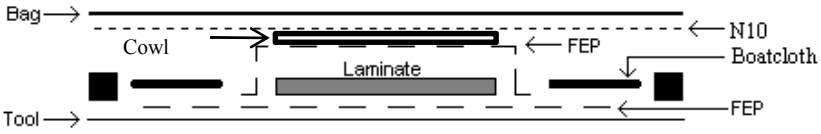

Figure 2-2 Bagging diagram for specimen

Specimen Layup Procedure

The specimen layup procedure is as follows:

1. Place Fluorinated ethylene propylene (FEP), a release film to prevent the polymer from bonding to the metal tooling during the cure process, on a smooth aluminum cure plate
2. Place carbon laminate the FEP covered cure plate
3. Lay a solid layer of FEP over laminate, sealed on all sides with FEP tape
4. Place edge breathers around the laminate
5. Place a cowl plate on top of the laminate
6. Place at least 3 thermocouples around the panel, under the edge breathers
7. Place boat cloth manifold around the laminate
8. Place a layer of N10 over entire panel to seal to cure plate with mud tape
9. Cover with bag and at least 2 vacuum ports and 1 probe port
10. Perform a leak check and ensure that over a 1 minute period no vacuum is lost

The final bagged part is now ready to be cured in the autoclave. Figure 2-3 shows the specimen undergoing a leak check before the final ports were installed.

Figure 2-3 Leak check performed on bagged laminate

Autoclave Curing

The last step to curing the specimen is to place the bagged carbon laminate inside an autoclave. Cure cycles and bagging procedures for composites is an art and is

often proprietary to the company that develops the technology. IM7-8552 is a common industry wide material and has many years of published bagging procedures and cure cycles. The cure cycle for this is shown below. Typically cure cycles are shown in a graphical form. This is because the autoclave records time, temperature, pressure, and vacuum and the results are displayed in a graphical form for documentation and analysis. Figure 2-4 shows the graphical form for the cure cycle. (8)

1. Apply full vacuum (at least 28” Hg)
2. Apply 100 PSI pressure
3. Remove vacuum at 30 PSI
4. Heat at 5°F/min to 365°F and hold at 355°F for 2 hours (345°F minimum)
5. Cool to Room Temperature at 4°F/min
6. Release pressure when laminate is below 150°F

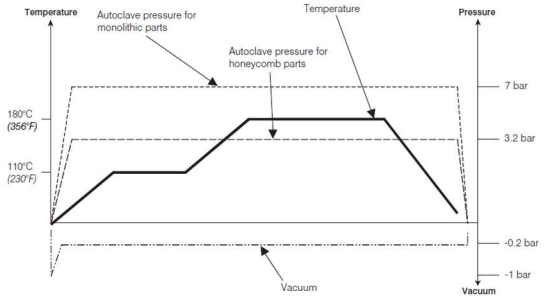

Figure 2-4 Curing cycle for IM7-8552

Figure 2-5 Specimen in autoclave

In order to cut the individual specimen to the correct size a wafer saw was used. The wafer saw uses deionized water for a lubricant and has a diamond blade that allows it to cut composites without splintering the material while maintaining a high tolerance.

Chapter 3

Flat Plate Torsion Method

With limitations of the ability of SBS to measure the nonlinear interlaminar shear stress-strain curve in the 2-3 plane the FPT test method was considered as a modified SBS test method. Digital image correlation (DIC) technique was used in conjunction with the FPT test method to experimentally determine the strains and FEA to calculate the stresses. The strains are determined experimentally using DIC and provide an initial approximation of strain for FEA to calculate the stresses. DIC is a noncontact test method to optically calculate full field strain during destructive testing. Strain gages have been used for years but are limited to local deformation at the location the sensor is installed. With the use of DIC it is possible to obtain full field strain profiles which are not possible with the use of strain gages alone. However, this technology is limited to surface deformation and must be visible to the cameras recording the data. A user defined subroutine, Umat is used to define the constitutive model for the FPT specimen. An iterative process is used to update the nonlinear properties using a best fit least square approximation method. The Ramberg-Osgood relationship provides a mathematical model to extract the nonlinear properties after each iteration which will be used as the initial approximation for the next iteration. Using regression analysis the root mean square error can be used to determine the difference in the stress-strain curve from the previous iteration. When the root mean square error is less than 3% the stress-strain curve is considered to be sufficiently converged and the final nonlinear properties are computed using the Ramberg-Osgood relationship.

Digital Image Correlation

DIC uses a system of cameras to optically measure the displacement of a specimen under load with respect to the x and y direction. Using the linear displacement

relationship in equation 1, where ε represents strain and L_o represents the original length before deformation,

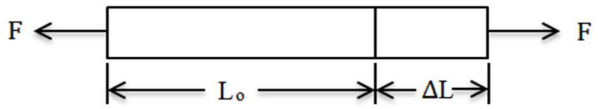

$$\varepsilon = \frac{\Delta L}{L_o} \tag{1}$$

DIC technique calculates the strain in the x and y direction using the relationship shown in equation 2, where ε_x is the strain with respect to the x direction and ε_y is the strain with respect to the y direction,

$$\varepsilon_x = \frac{\partial U_x}{\partial x}, \ \varepsilon_y = \frac{\partial U_y}{\partial y} \tag{2}$$

from a series of photographs throughout the testing process. The photographs serve as time points during the loading process and make it able to correlate FEA to a load during testing. A speckle pattern is applied to the specimen in order to optically measure the elongation of the specimen be tracking the displacement of particles in comparison to an unstressed state. Two cameras are necessary for each surface you are trying to measure. In this test two 16 megapixel Proscilla GE cameras were used to measure strain in the 1-3 and 2-3 plane simultaneously. Figure 3-1 shows a typical setup of DIC ready for testing. The specimens need to have a pattern painted on the surface that is intended to be measured. The pattern is applied with a detailed air brush kit. A strong contrast between the background and pixel color is favorable. The specimen is painted with a flat white coat and then speckled with black. Figure 3-2 shows a FPT specimen prepared for testing using a speckle pattern.

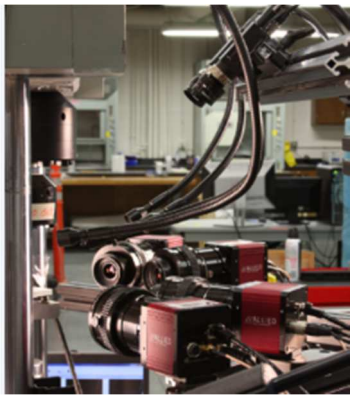

Figure 3-1 Typical DIC camera setup

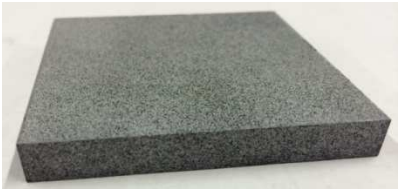

Figure 3-2 FPT specimen prepped for testing

The speckle pattern allows for the cameras to use pattern recognition software to track the change of the specimen during the test. This occurs by first syncing the left and right camera to focus on the same spot called a subset. In each subset 3 color changes are optimum for the DIC software to recognize each subset independently. VIC-3D software was used in the FPT testing for this research. Figure 3-3 shows the subset in the left camera being recognized in the right camera. (10) The angle between the cameras provides the necessary alignment to calculate the strain. A camera angle of 25 to 35 degrees is optimum for best resolution between the cameras.

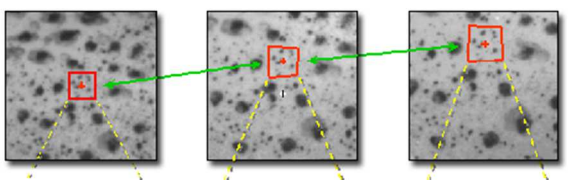

Figure 3-3 DIC subset recognition in the left and right cameras

The data is collected by a series of photographs that are taken throughout the test that will be used to correlate load points with FEA. Each photograph is then linked to the previous one. As the specimen deforms the speckle pattern deforms with the specimen and provides the strain and out of plane displacement. The first camera shot is assumed to be at zero deformation and is taken before the testing begins and serves as the reference length. All further shots are compared to this zero shot and the data is calculated. The results are displayed in a similar fashion to a FEA model shown in Figure 3-4. Each facet is similar to a node in a finite element model and strain and deformation data can be obtained for each one. For the flat plate torsion test setup a facet size of 45 x 45 pixels was used, which corresponds to 0.47 mm^2 and is also the equivalent strain gage measurement area. (5) This correlates to about 20,000 data points per load step.

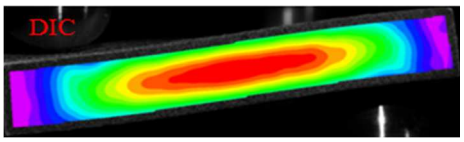

Figure 3-4 Typical strain output from DIC

Flat Plate Torsion Test Method Setup

A modified SBS test method was used to prevent the axial strain from causing tensile failure due to bending in the 2-3 plane before the curve becomes nonlinear. The flat plate torsion test was considered due to the loading configuration being different then SBS. The axial stresses are an order of magnitude less than the shear stress using the FPT test method however, some tension still exists but it is not as significant as the shear strain allowing the specimen to undergo larger shear strains before failure. The FPT test method puts a large volume of the specimen under shear stress which is good when trying to measure the nonlinear interlaminar shear strain in the 2-3 plane. Spherical loading surfaces were placed on the opposite upper and lower surfaces of a flat plate

carbon specimen. Careful consideration to the diameter of the contact surfaces was considered to prevent stress concentrations from loading and causing the specimen to fail in compression due to the supports. SBS research has shown that if the diameter is too small the specimen will fail in compression due to the contact supports, and when the intention is to measure shear strain the ideal test would need to undergo pure shear. The FPT concept is illustrated in Figure 3-5.

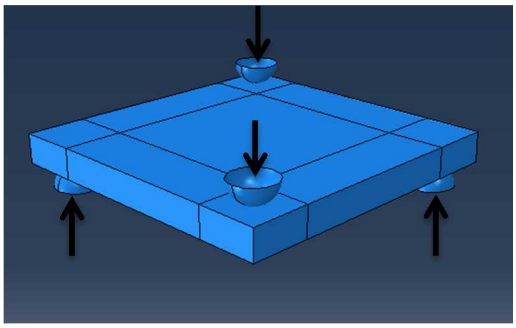

Figure 3-5 Flat plate torsional loading concept

Using a MTS static test machine and a 2000 lb. load cell the specimen is loaded in compression at 0.05 in./min crosshead displacement rate to create a torsional deformation until failure of the specimen occurs. Different contact surfaces were considered to examine the effects they would have on the specimen during testing and to reduce the stress concentrations the loading surfaces created. The diameters for these tests were specifically chosen to be larger than that of the SBS test to reduce the stress concentrations caused by contact surfaces. Additionally spherical and cylindrical supports were both considered to determine the sensitivity of the location of the contact surfaces. The specimen geometry was modified to assess different test configurations and the ability for the specimen to undergo a large amount of shear strain before the specimen exhibited failure. Studies have shown that the s/t have a strong influence on the “apparent shear strength” and the failure modes of the SBS specimen. In general as

the s/t decreases from 4 the supports began to be directly under the loading surface causing the specimen to fail due to compression or crushing of the contact surfaces resulting from increased stress concentrations. As s/t increases large enough the specimen is no longer a short beam and tensile or compressive failures will occur.

Initially a thickness of 0.25" was chosen similarly to SBS in order to be able to machine SBS and FPT specimen from the same panel. A 2.0" support span, determined from the s/t ratio of 8, was chosen based on similar FPT testing and historical SBS data showing an s/t ratio in that range was sufficient. ASTM D2344 suggests that a length corresponding to the thickness of the specimen be added to the overall specimen length on either side of supports. Using the 0.25" specimen this increased the overall length of the first FPT specimen to 2.5" with a support span of 2.0" and a thickness of 0.25". Spherical loading surfaces were initially used similarly to SBS tests and the diameter of these were chosen to be 0.375" which are larger than that of SBS to possibly reduce the stress concentrations the contact supports cause. They were chosen such that they were not too large to block DIC from getting data in the principal planes and that they were not too small such to create stress concentrations. The diameter was chosen from standard off the shelf parts such that the diameter of the contact surfaces could easily be replaced with another off the shelf part if necessary.

A 0.16" thick specimen was also considered similar to previous testing of a modified SBS specimen. A specimen thickness of 0.167" was determined based on the cured ply thickness of each ply being 0.0065" and wanting an even number of laminates closest to 0.16". An s/t ratio of 4 was determined to be similar to SBS specimen and using similar methodology as previously mentioned the overall length of the specimen was chosen to be 1.0" with a support span of 0.7". The diameters to test the 1" specimen were chosen for the same methodology previously stated to be 0.25" and 0.375". The

tabulated list of the different specimen geometry and contact surfaces used in this research is shown in Table 3-1 and the test configurations are illustrated in Figure 3-6.

Table 3-1 Flat plate torsion test configurations

Distance between contacts	Length	Width	Thickness	Contact Type	Contact Diameter
2.0”	2.5”	2.5”	0.25”	Spherical	0.375”
0.7”	1.0”	1.0”	0.167”	Spherical	0.375”
0.7”	1.0”	1.0”	0.167”	Spherical	0.25”
0.7”	1.0”	1.0”	0.167”	Cylindrical	0.25”

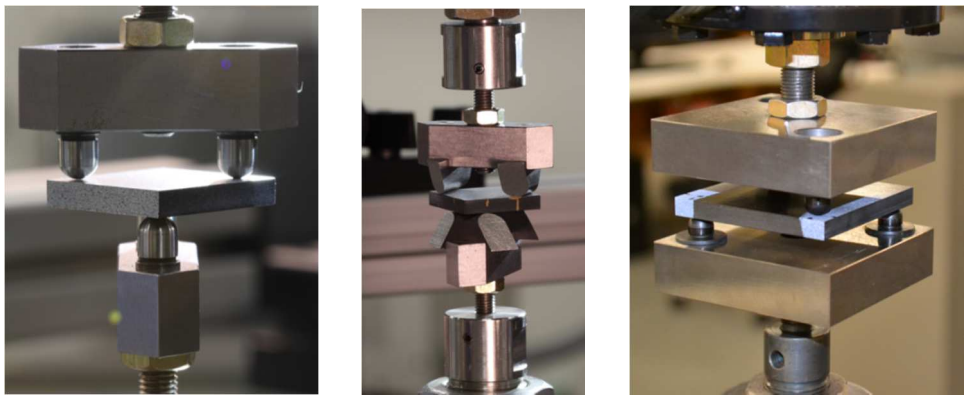

Figure 3-6 FPT test setup configurations

Multiple test fixtures had to be machined for each different test setup. An upper and lower fixture was fabricated to the fit the MTS test fixture crossheads. Each piece was threaded to the crosshead for testing. The loading surfaces were machined from hardened steel. Figure 3-7 shows the machined test fixtures for the spherical and cylindrical contact surfaces.

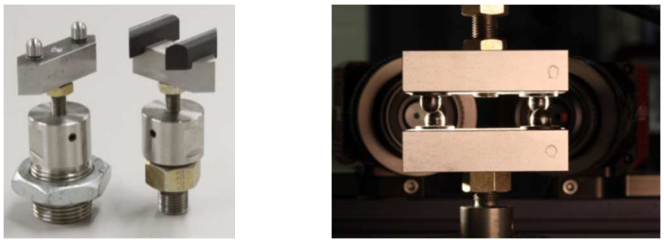

Figure 3-7 Contact supports for FPT test

In order to ensure the loading surfaces are symmetric and the loading is normal to the specimen an alignment tool was used to align the test machine before testing. A pocketed middle plate was used to align off of the contact surfaces by lowering the crosshead until the contact surfaces sat inside the pockets, or grooves shown in Figure 3-8. Once the upper and lower crosshead was aligned the nut on the test fixture was tightened so that when the fixture alignment tool was removed the crosshead would remain in place. Once the test stand is aligned the center alignment block was removed and the specimen was installed. The specimen was placed in between the test fixture and the top is lowered until contact is made between the upper and lower plates and the specimen.

Figure 3-8 FPT fixture alignment tools and setup

Alignment tools were also used to center the specimen in the test fixture. Using a specimen alignment tool shown in Figure 3-9, each specimen was loaded to ensure the specimen was being loaded symmetrically.

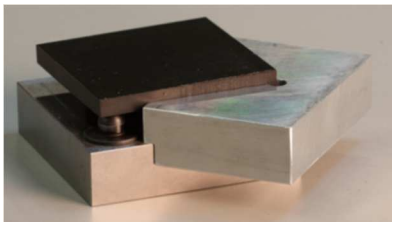

Figure 3-9 FPT specimen alignment tool

With the alignment tool in place the crosshead was lowered until the specimen came in contact with the contact surfaces. After the specimen was secure in the test

fixture the specimen alignment tool was removed and the specimen was ready for testing. Once the fixture is aligned and ready to test the loading arms apply a load in compression until failure occurs. Figure 3-10 shows a 2.5" square FPT specimen under load.

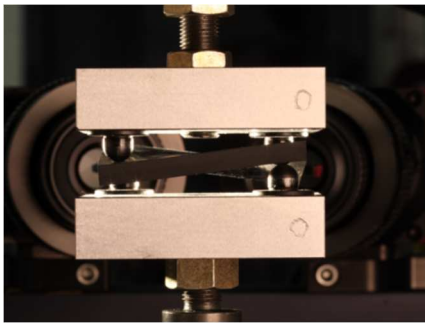

Figure 3-10 2.5" square FPT specimen under load

Finite Element Analysis

The specimens were modeled in Abaqus, a FEA software program. The C3D8I elements are ideal for the torsion and bending the FPT test methods presents. The carbon specimens were modeled using a C3D8I mesh which is practical for solid rectangular elements. The supports were modeled as analytic rigid solids and the assumption is that they do not deform during testing. Hardened steel, commonly used in static and fatigue test fixtures of carbon composites was used to fabricate the contact surfaces to represent a non-deformable surface as modeled in FEA.

Flat Plate Torsion Test Specimen Mesh

The C3D8I mesh describes the five aspects of the elements in the mesh. These are the family, the degrees of freedom, number of nodes, formulation, and integration. (11) A continuum element was chosen due to its common use for solid and fluid elements and represents and rectangular element with nodes at each of the corners. Figure 3-11 shows a typical continuum element with an 8-node brick style node placement. (11)

Eight node rectangular elements represent a linear solution with integrated stresses and strains within the element. An incompatible mode element is a first-order element that is enhanced to improve bending behavior. (11) These are added internally to the elements to eliminate parasitic shear stresses that cause the response to be too stiff in bending. Incompatible mode elements also eliminate artificial stiffening that is caused by Poisson's effect in bending when approximately incompressible materials are considered. (11)

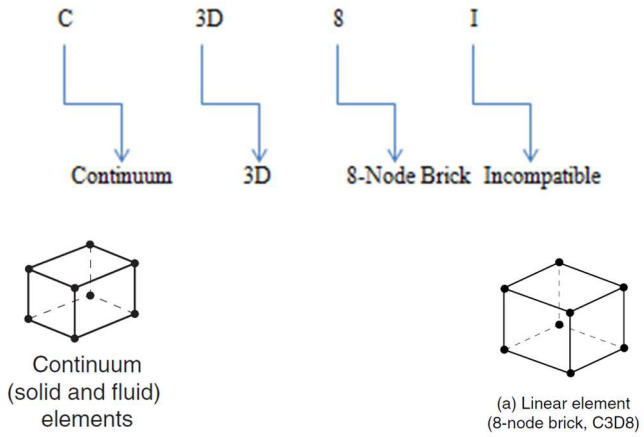

Figure 3-11 Typical continuum element family (left) Typical 8-node brick model (right)

The specimen was partitioned in 4 quadrants to use a more detailed mesh at the corner where stress concentrations occur due to the contact surfaces. By doing so the number of elements could be increased at the corners and not in the center where no contact stresses occur. This is to reduce the amount of processing time to run the analysis for each test since a less defined mesh is sufficient in the center of the specimen where no contact is occurring. The elements use to generate the mesh were labeled as the s_i, s_o, and s_t as shown in Figure 3-12.

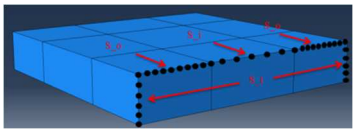

Figure 3-12 Elements used to model FPT specimen

Figure 3-13 shows the mesh generated for the FPT specimen in this research. The regions defined by the different elements show a more refined mesh in the corners where stress concentrations occur.

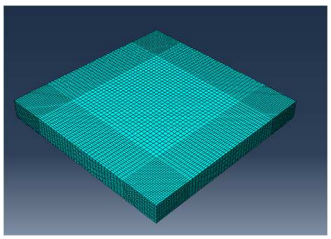

Figure 3-13 Regions created using a partitioned C3D8I mesh in Abaqus

The contact surfaces were modeled as frictionless analytic rigid surfaces. Two types of surfaces were considered in the FPT, spherical and cylindrical. In Abaqus an analytic rigid surface is a geometric surface whose motion is governed by a reference node. This made it convenient to represent the loading of the FPT test fixture and a surface to surface contact formulation was used in order to not have local indentation stresses from the contact points. Figure 3-14 shows the different surfaces considered in the FPT.

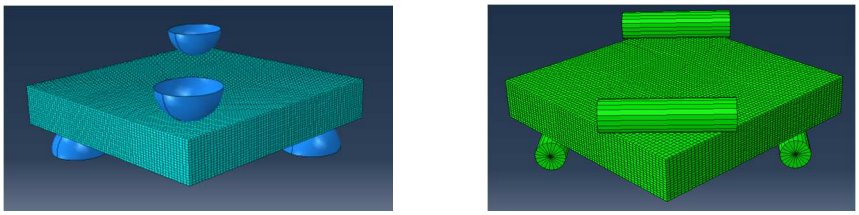

Figure 3-14 Specimen and contact surface mesh assembly

Mesh Convergence

In order to ensure a proper stress convergence was achieved a mesh convergence study was conducted. To determine the sensitivity of the mesh elements, s_i, s_t, and s_o the elements were increased until the change in $\sigma_{23\ max}$ converged to a steady state. Due to computation time and computer space an over meshed model is not

favorable. In the thickness direction it was determined that 16 elements were sufficient to ensure stress convergence and a strong stress gradient. Figure 3-15 shows the stress convergence results from the mesh convergence sensitivity analysis. (5)

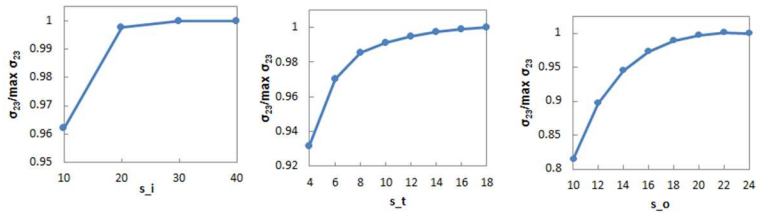

Figure 3-15 Mesh convergence sensitivity analysis

Stress Formulations

The constitutive stress-strain relationship for an orthotropic composite material can be characterized by Equation 3; however it needs to be modified to capture the shear non-linearity.

$$\begin{bmatrix}\epsilon_{11}\\ \epsilon_{22}\\ \epsilon_{33}\\ \gamma_{12}\\ \gamma_{13}\\ \gamma_{23}\end{bmatrix} = \begin{bmatrix} \frac{1}{E_1} & -\frac{\nu_{21}}{E_2} & -\frac{\nu_{31}}{E_3} & 0 & 0 & 0 \\ -\frac{\nu_{12}}{E_1} & \frac{1}{E_2} & -\frac{\nu_{32}}{E_3} & 0 & 0 & 0 \\ -\frac{\nu_{13}}{E_1} & -\frac{\nu_{23}}{E_2} & \frac{1}{E_3} & 0 & 0 & 0 \\ 0 & 0 & 0 & \frac{1}{G_{12}} & 0 & 0 \\ 0 & 0 & 0 & 0 & \frac{1}{G_{13}} & 0 \\ 0 & 0 & 0 & 0 & 0 & \frac{1}{G_{23}} \end{bmatrix} \begin{bmatrix}\sigma_{11}\\ \sigma_{22}\\ \sigma_{33}\\ \tau_{12}\\ \tau_{13}\\ \tau_{23}\end{bmatrix} \quad (3)$$

The FEM accounts for the geometric nonlinearity and the material shear nonlinearity is implemented using a subroutine UMAT. (5) A nonlinear shear stress-strain relationship was characterized using a log-linear relationship, the Ramberg-Osgood relationship, shown in Equation 4 containing 3 material parameters G, K, and n; where G is the linear shear modulus, K is the secant-intercept modulus, n is the exponential material constant, and γ and τ are the shear strain and shear stress.

$$\gamma = \left(\frac{\tau}{G}\right) + \left(\frac{\tau}{K}\right)^{\frac{1}{n}} \tag{4}$$

$$\gamma_{23} = \left(\frac{\tau_{23}}{G_{23}}\right) + \left(\frac{\tau_{23}}{K_{23}}\right)^{\frac{1}{n_{23}}} \tag{5}$$

$$\gamma_{13} = \left(\frac{\tau_{13}}{G_{13}}\right) + \left(\frac{\tau_{13}}{K_{13}}\right)^{\frac{1}{n_{13}}} \tag{6}$$

Equation 4 can be utilized to calculate the strain in each principal plane however in this research ε is determined experimentally and σ needs to be calculated. Equation 4 cannot directly be solved for σ, but it can be used to derive the incremental expression for the Jacobian compliance matrix shown in Equation 7.

$$[J] = \frac{\partial \Delta \varepsilon}{\partial \Delta \sigma} \tag{7}$$

Equation 7 can be inverted to get the Jacobian stiffness matrix shown in Equation 8.

$$J = \frac{\partial \Delta \sigma}{\partial \Delta \epsilon} = \left[\frac{\partial \Delta \epsilon}{\partial \Delta \sigma}\right]^{-1} \tag{8}$$

UMAT can use the analytical expression of the Jacobian stiffness matrix in Equation 8 to define the constitutive model in the FEM and calculate the shear stress. The location of max shear strain from DIC is used to compute the shear stresses as shown in Figure 3-16.

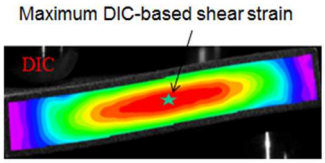

Figure 3-16 - Location of max shear strain from DIC

Material Property Assumptions

The initial nonlinear material properties for G, K, and n for the 1-2 and 1-3 planes were based off SBS tests and were used to define shear material behavior where G_{12} = G_{13} = 5.08 Gpa (0.737 msi), k_{12} = k_{13} = 0.249 Gpa (36.1 ksi), and n_{12} = n_{13} = 0.248. The

initial approximations for Young's moduli were assumed as E_{11} = 157 Gpa (22.7 msi) and E_{22} = E_{33} = 8.96 Gpa (1.3 msi) and v_{12} = v_{13} = 0.32 and v_{23} = 0.5 were used for the initial assumptions for Poisson's ratio. Initial approximations for the shear modulus G_{23} were assumed using transverse isotropy shown in equation 8,

$$G_{23} = \frac{E_{23}}{2(1+\nu_{23})} \tag{8}$$

Where G_{23} = 2.99 Gpa (0.422 msi). Initial approximations for the nonlinear material shear properties for K and n in the 2-3 plane are k_{23} = 0.147 Gpa (21.3 ksi) and n_{23} = n_{13} = n_{12} = 0.248. K_{23} was initially estimated using a ratio between G and K already determined as seen in equation 9.

$$\frac{K_{23}}{K_{13}} = \frac{G_{23}}{G_{13}} \tag{9}$$

Table 3-2 shows the material properties in tabular form that were used as the initial material properties for this research. (5) A sensitivity analysis was conducted to determine how sensitive FPT test method and stress calculations were to initial assumptions. The results showed that the final stress-strain curve was not affected by the initial properties and only caused the iteration process to have more iteration before convergence. (5)

Table 3-2 Material property initial assumptions

Material Property	Initial Assumption
E_{11}	157 Gpa (22.7 msi)
E_{22}	8.96 Gpa (1.3 msi)
E_{33}	8.96 Gpa (1.3 msi)
v_{12}	0.32
v_{13}	0.32
v_{23}	0.5
G_{12}	5.08 Gpa (0.737 msi)
G_{13}	5.08 Gpa (0.737 msi)
G_{23}	2.99 Gpa (0.433 msi)
K_{12}	0.249 Gpa (36.1 ksi)
K_{13}	0.249 Gpa (36.1 ksi)
K_{23}	0.147 Gpa (21.3 ksi)

Table 3-2 – Continued

$\mathbf{n_{12}}$	0.248
$\mathbf{n_{13}}$	0.248
$\mathbf{n_{23}}$	0.248

Stress Convergence and Nonlinear Property Calculations

A log-linear stress-strain curve is generated from FEA calculated stresses and DIC max shear strains obtained experimentally using the loads points from DIC to sync the stresses and strains to the same load. The nonlinear properties G_{23}, K_{23}, and n_{23} were determined using a least square approximation method by using a best fit comparison of the data points and were updated into FEA for the next iteration. A normalized root-mean square error approximation is used to calculate the percent change in the stress from previous iterations and was used to end the iteration processes once a convergence criterion was met. Using the root-mean square approximation relationship shown in Equation 8, where ε is the normalized root-mean square error approximation,

$$\varepsilon = \sqrt{\frac{1}{N}\sum_{i=1}^{n}\left\{\left[\frac{\sigma_i^{k+1} - \sigma_i^{k}}{\sigma_i^{k+1}}\right]^2\right\}} \tag{8}$$

σ_i is the max shear stress at each load step, and N is the number of load steps that were generated from DIC. When less than a 3% change in stress from one iteration to the next was calculated the iterative processes was stopped. Depending on the how far off the initial material property assumptions were determined the amount iterations involved. For this research typically 4-5 iterations were required satisfy the convergence criterion. The process is shown graphically in Figure 3-17.

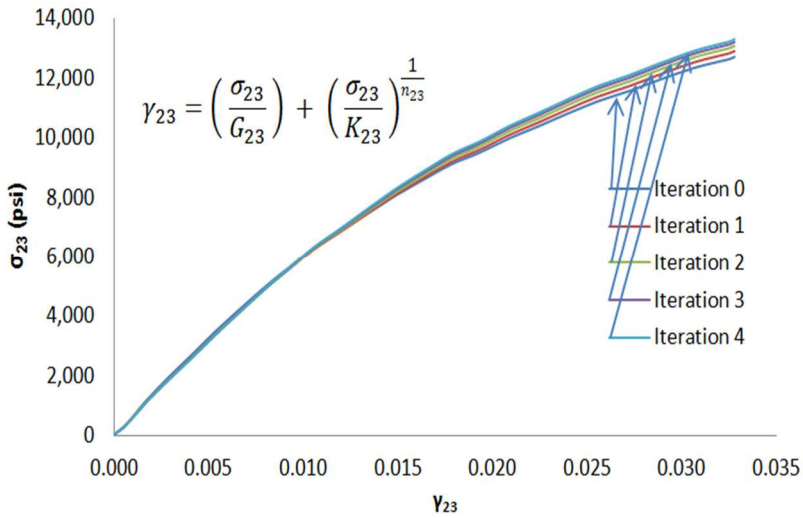

Figure 3-17 Typical shear stress-strain convergence

Chapter 4

Flat Plate Torsion Test Results

Testing was conducted in the Advanced Materials and Structures Lab at the University of Texas Arlington at room temperature. The specimens were prepped for DIC with a speckle pattern and were identified uniquely. Each specimen was measured and documented before each test. Four unique test configurations were considered and tested all using unidirectional carbon composites IM7-8552 including a 2.5" square specimen with 0.375" spherical contact surfaces, a 1" square specimen 0.167" thick with 0.25" contact surfaces, a 1" square specimen 0.167" thick with 0.375" contact surfaces, and a 1" square specimen 0.167" thick with 0.25" cylindrical contact surfaces.

2.5" Square Flat Plate Torsion Tests with Spherical Contact Surfaces

Initially a 2.5" square carbon specimen 0.25" thick was tested. The contact surfaces were spherical balls made of hardened steel 0.375" in diameter. These specimens were fabricated using 38 unidirectional plies to achieve the 0.25" thickness. After testing and experimentally measuring the shear strains form DIC the shear stresses were calculated for each specimen and then plotted together. Figure 4-2 shows the nonlinear interlaminar shear stress-strain curve in the 2-3 plane. The specimen exhibited similar peak loads and all failed near 990 lbs. and 3 % shear strain in the 2-3 plane. Figure 4-1 shows the test fixture used to test the 2.5" specimen and the typical failure of each specimen. Typical failure occurred at the mid plane of the specimen in the fiber direction.

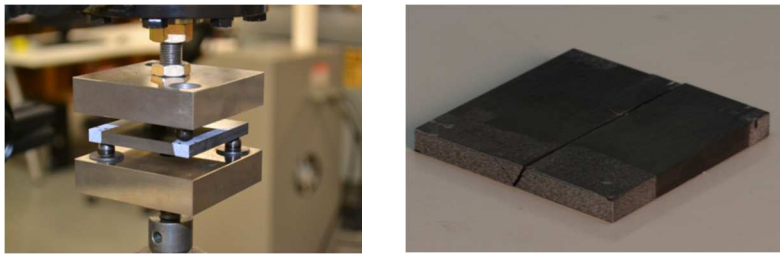

Figure 4-1 FPT 2.5” test fixture (left), and typical failure for 2.5” FPT specimen (right)

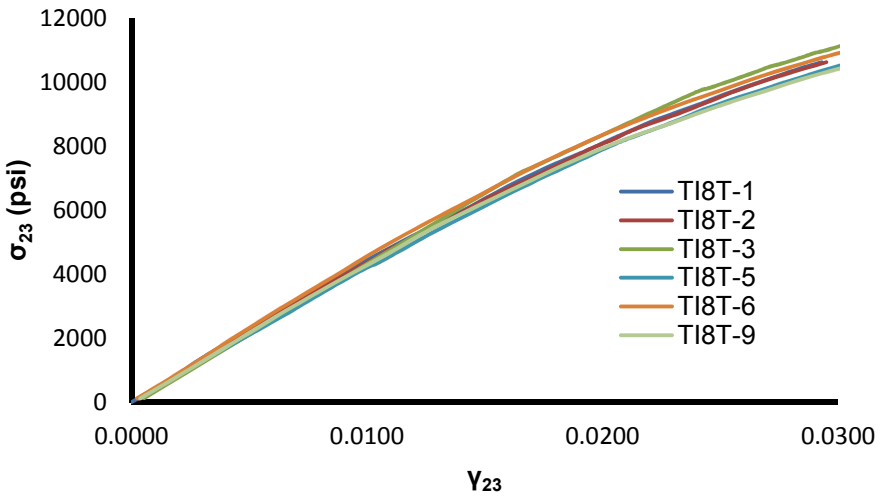

Figure 4-2 FPT interlaminar shear stress-strain curve for 2.5” specimen in 2-3 plane

The curve from the 2.5” square specimen in the 1-3 plane was plotted with existing SBS data to validate the 2-3 plane. The SBS curve used is from published data on unidirectional carbon specimen. (12) Both the 2.5” carbon specimen and the existing SBS curve showed a matching trend and Figure 4-3 shows the 2 curves.

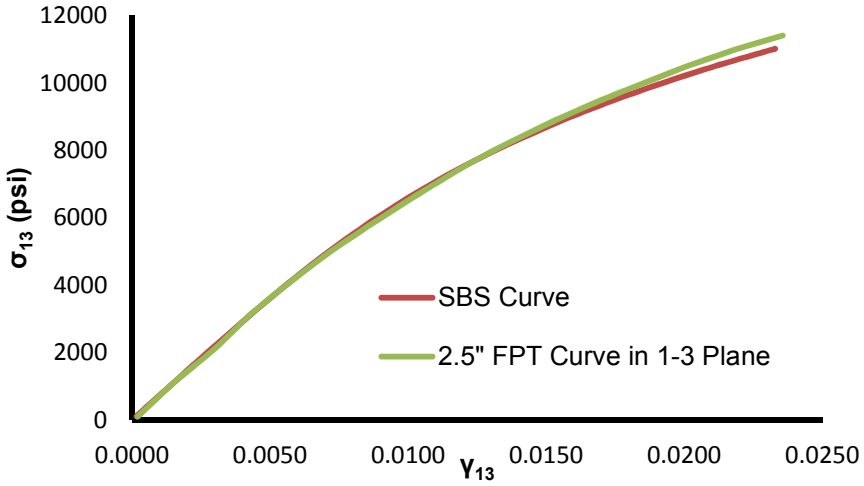

Figure 4-3 SBS curve and 2.5" FPT curve in 1-3 plane

The nonlinear properties for these test were calculated using the nonlinear and linear logarithmic methods shown in Table 4-1. Figure 4-4 shows the FEM shear strains and the DIC experimental shear strains for both the 1-3 and 2-3 plane. The strain relationship between DIC and FEA both display similar strain patterns and values. (5)

Table 4-1 Summary of nonlinear properties from FPT 2.5" specimen in 2-3 plane

	Nonlinear Method			**Linear Logarithmic Method**		
	G	**K**	**N**	**G**	**K**	**N**
TI8T-1	450566	41678	0.264	443380	38881	0.247
TI8T-2	442919	38851	0.249	436370	38165	0.240
TI8T-3	439350	25070	0.153	409016	18782	0.090
TI8T-5	420931	31854	0.210	419850	31946	0.209
TI8T-6	459993	33876	0.224	448179	28470	0.187
TI8T-9	435537	33532	0.230	438715	37654	0.251
Average	441549	34143	0.22	432585	32316	0.20

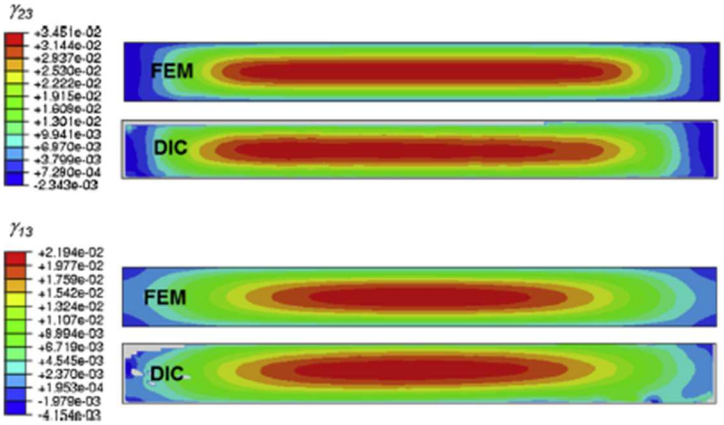

Figure 4-4 DIC and FEM shear strain for 2.5" FPT specimen at peak load

1.0" Square Flat Plate Torsion Tests with Spherical Contact Surfaces

A 1" square specimen with a thickness of 0.167" was tested. The 1" FPT specimens were tested with 0.25" and 0.375" spherical contact surfaces in order to determine the sensitivity of the diameter of the contact surfaces. The contact surfaces were made from hardened steel. The specimen was fabricated using 26 plies to achieve the 0.167" thickness. Figure 4-5 shows the test fixture used for the 1" FPT specimen and the typical failure. Typical failure of the 1" specimen typically occurred at the mid-plane of the 2-3 plane along the fiber direction.

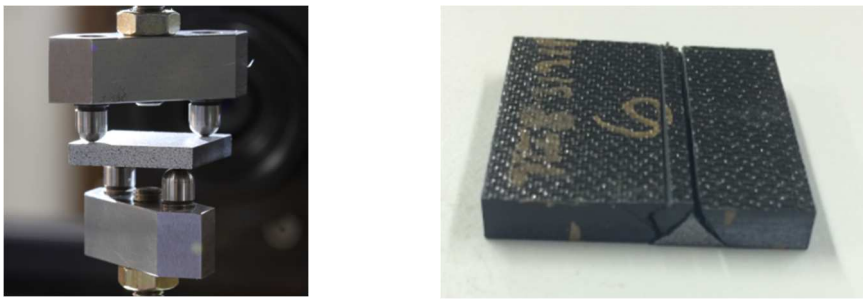

Figure 4-5 1" FPT test fixture (left) and typical 1" FPT specimen failure (right)

Figure 4-6 and Figure 4-7 shows the nonlinear shear stress-strain curves for the 2-3 and 1-3 plane. The shear strain reached 5% in the 2-3 plane and 3.5% in the 1-3 plane. The average load of failure was 600 lbs. and the average max shear stress was 14000 psi.

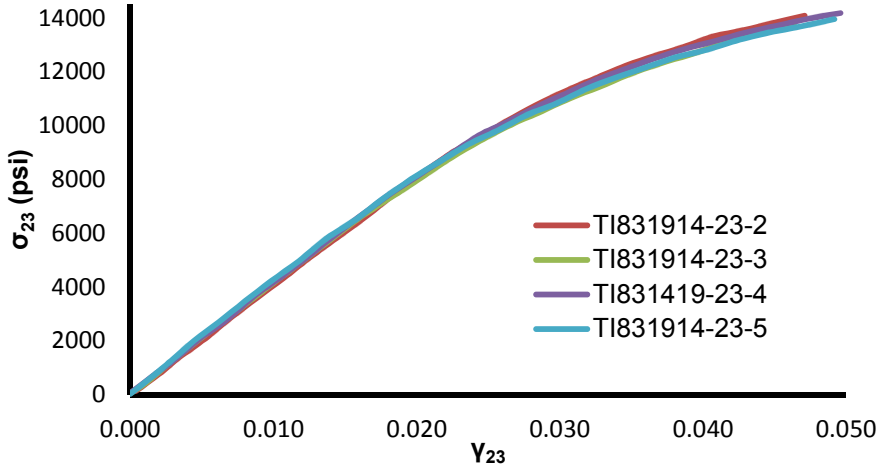

Figure 4-6 FPT interlaminar shear stress-strain curve for 1.0" specimen in 2-3 plane with 0.25" spherical contact surfaces

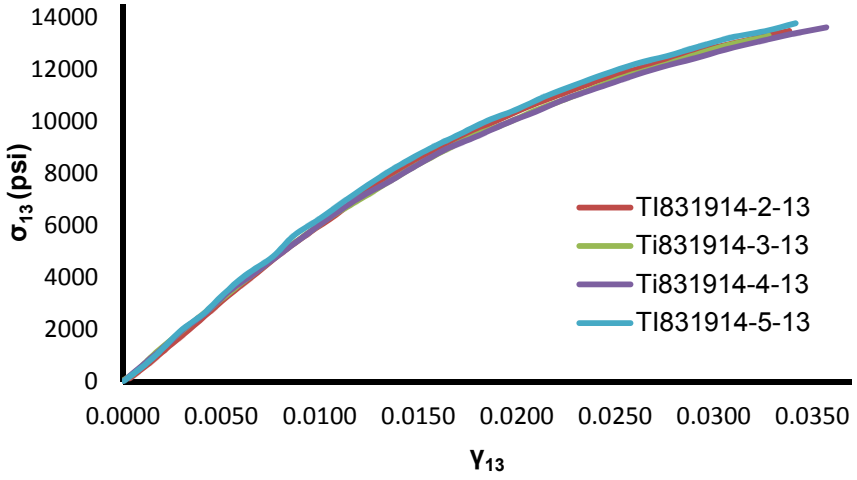

Figure 4-7 FPT interlaminar shear stress-strain curve for 1.0" specimen in 1-3 plane with 0.25" spherical contact surfaces

The 1” FPT specimen were tested using the 0.375” contact surfaces. Figure 4-8 shows the stress-strain curves for the 1” FPT specimen with 0.375” spherical contacts compared to 1” FPT specimen 0.25” spherical contact surfaces. The difference in the curves with for the 0.375” diameter and the 0.25” diameter were less than 1%. The max shear strain for both 1-3 an 2-3 plane was typically 10% less using the larger diameter contact surfaces.

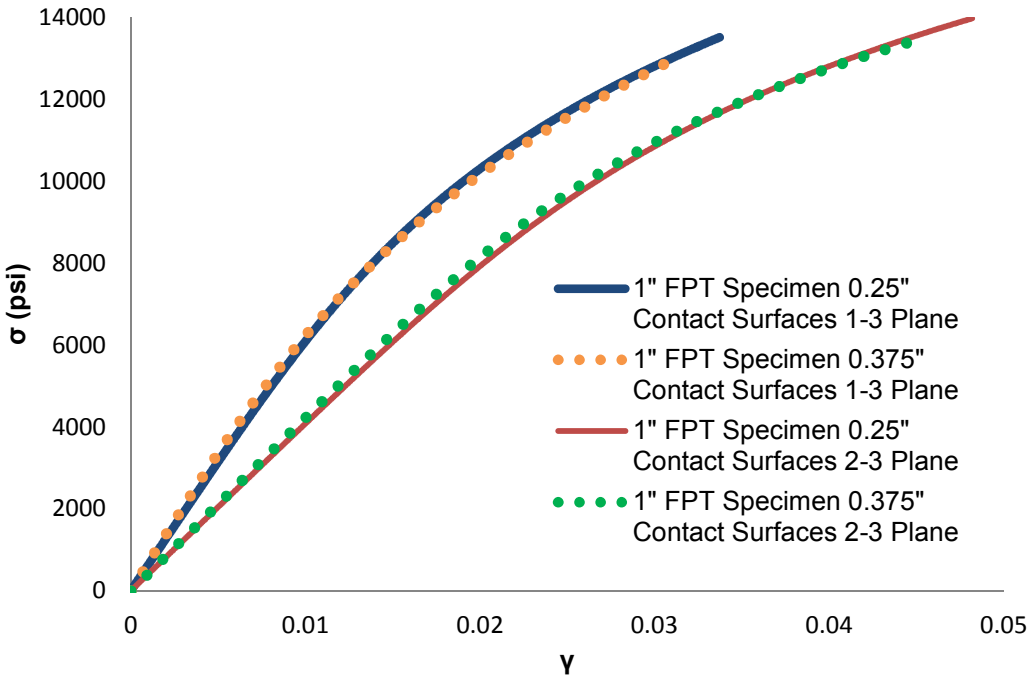

Figure 4-8 1” FPT specimen with spherical contact surfaces in the 1-3 and 2-3 plane

Table 4-2 shows the tabulated results for the nonlinear properties for the 2-3 plane and

Table 4-3 shows the results in the 1-3 plane.

Table 4-2 Summary of nonlinear properties from FPT 1.0” specimen in 2-3 plane with spherical contact surfaces

	Nonlinear Method			Logarithmic Linear Method		
	G	**K**	**N**	**G**	**K**	**N**
TI831914-23-2	406203	26097	0.140	409377	34573	0.191
TI831914-23-3	416250	31246	0.193	413991	27801	0.167
TI831914-23-4	414420	26889	0.152	410716	25634	0.142
TI831914-23-5	423731	29236	0.179	428226	33964	0.211
Average	407709	27499	0.163	408952	30304	0.181

Table 4-3 Summary of nonlinear properties from FPT 1.0” specimen in 1-3 plane with spherical contact surfaces

	Nonlinear Method			Logarithmic Linear Method		
	G	K	N	G	K	N
TI831914-13-2	611521	31585	0.192	660478	42983	0.277
TI831914-13-3	637056	41299	0.256	669359	43783	0.284
TI831914-13-4	628998	36831	0.233	687065	42914	0.289
TI831914-13-5	650451	35677	0.219	665643	43607	0.289
Average	632007	36348	0.225	670636	43322	0.280

The strains from FEM were compared to the strains of DIC and are represented in Figure 4-9 and Figure 4-10. Both strain patterns exhibited similar strain results and peak strains.

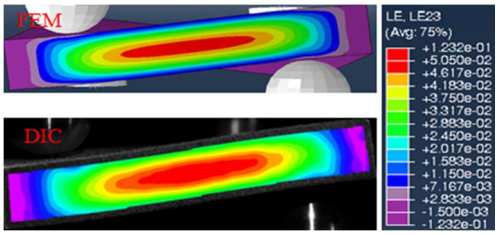

Figure 4-9 DIC and FEM shear strain comparison for 1.0” FPT specimen at peak load in 2-3 plane

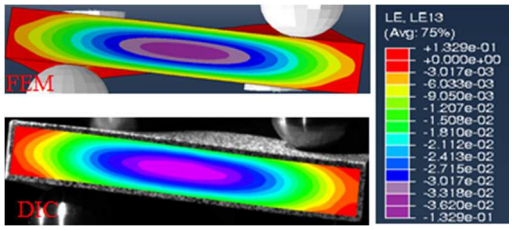

Figure 4-10 DIC and FEM shear strain comparison for 2.5" FPT specimen at peak load in 1-3 Plane

1.0" Square Flat Plate Torsion Tests with Cylindrical Contact Surfaces

1" FPT specimen 0.167" was tested using hardened steel cylindrical contact surfaces. Figure 4-11 shows the test fixture used to test these specimen and a typical failure for these specimen. Failure for these specimens typically occurred at the edge of the specimen due to crushing from the contact surfaces. Failure was initiated in the 2-3 plane along the fiber direction near the cylindrical contact surfaces.

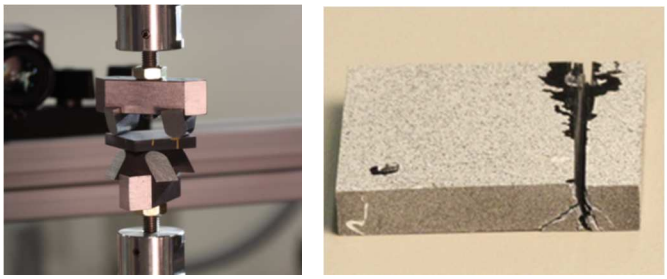

Figure 4-11 1.0" FPT with cylindrical contact surfaces (left) and typical failure (right)

The interlaminar shear stress-strain curves for the 1" FPT specimen with 0.25" cylindrical contact surfaces is shown in Figure 4-12 for the 2-3 plane and Figure 4-13 for the 1-3 plane.

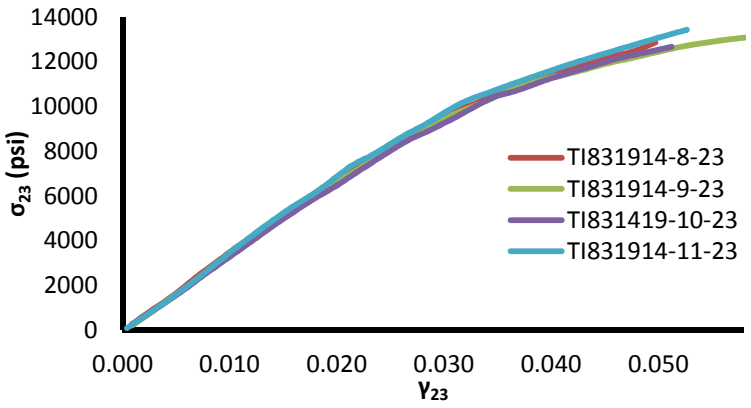

Figure 4-12 FPT interlaminar shear stress-strain curve for 1.0" specimen in 2-3 plane with 0.25" cylindrical contact surfaces

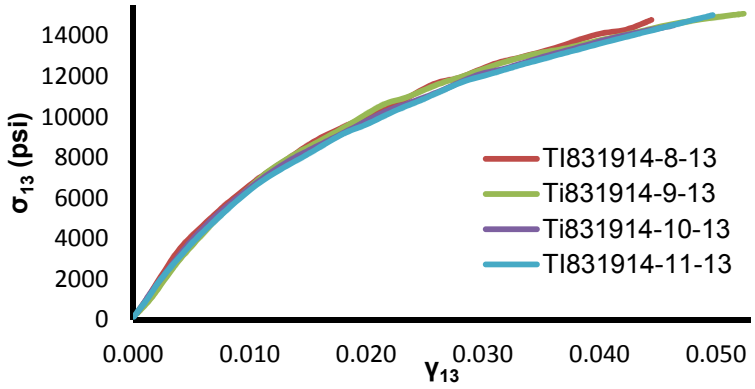

Figure 4-13 FPT interlaminar shear stress-strain curve for 1.0" specimen in 1-3 plane with 0.25" cylindrical contact surfaces

Table 4-4 and Table 4-5 show the nonlinear properties calculated for the 1" FPT specimen with 0.25" cylindrical contact surfaces.

Table 4-4 Summary of nonlinear properties for 1” specimen with 0.25” cylindrical contact surfaces in the 2-3 plane

	Nonlinear Method			Logarithmic Linear Method		
	G	**K**	**N**	**G**	**K**	**N**
TI831914-8-23	346088	28805	0.186	346724	30339	0.196
TI831914-9-23	334096	22561	0.136	350245	30580	0.208
TI831914-10-23	327434	23953	0.145	341227	30437	0.201
TI831914-11-23	349005	28940	0.181	356632	30539	0.210
Average	341430	26387	0.162	353612	30841	0.204

Table 4-5 Summary of nonlinear properties for 1” specimen with 0.25” cylindrical contact surfaces in the 1-3 plane

	Nonlinear Method			Logarithmic Linear Method		
	G	**K**	**N**	**G**	**K**	**N**
TI831914-8-13	880295	47067	0.324	736901	44363	0.297
TI831914-9-13	691106	33294	0.225	736449	46042	0.273
TI831914-10-13	814621	43305	0.306	734905	45085	0.293
TI831914-11-13	800905	45056	0.317	733129	43046	0.299
Average	796732	42181	0.293	735346	44634	0.290

The strain patterns for the cylindrical supports created a different strain pattern then the other test methods due to edge loading of the contact surfaces. The strains from FE were verified from DIC and are shown in Figure 4-14 and Figure 4-15. The location of max strain was not in the center of the 2-3 plane as in previous testing and was at the location of the contact supports.

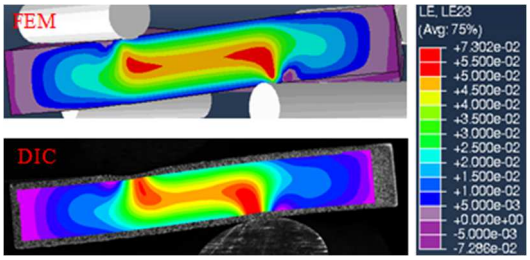

Figure 4-14 DIC and FEM shear strain comparison for 1.0" FPT specimen at peak load in the 2-3 plane

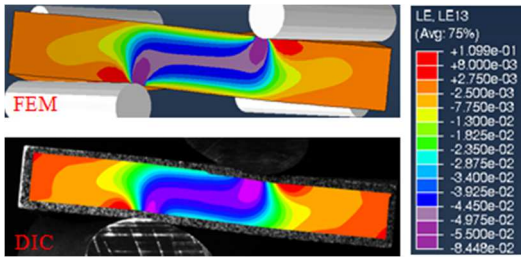

Figure 4-15 DIC and FEM shear strain comparison for 1.0" FPT specimen at peak load in the 1-3 plane

Table 4-6 shows the summary of the average and peak stresses, strains, and loads for all by test method. A summary of the nonlinear properties is shown in Table 4-7.

Table 4-6 Summary of FPT average and peak values by test

Contact Surfaces	Plane	L x W	T	Avg Stress	Avg Strain	Avg Load	Peak Stress	Peak Strain	Peak Load
0.25 Spherical Contacts	2-3	2.5	0.25	10675	0.03	973	10960	0.031	995
	1-3	2.5	0.25	11954	0.023	989	12501	0.023	995
0.25 Spherical Contacts	2-3	1.0	0.167	13989	0.047	597	14188	0.049	609
	1-3	1.0	0.167	13533	0.034	597	13763	0.035	609
0.25 Cylindrical Contacts	2-3	1.0	0.167	13438	0.052	653	13438	0.052	653
	1-3	1.0	0.167	15018	0.049	653	15018	0.049	653
0.375 Spherical Contacts	2-3	1.0	0.167	12300	0.045	554	12300	0.045	554
	1-3	1.0	0.167	12300	0.03	554	12300	0.03	554

Table 4-6 – Continued

Published	2-3	2.5	0.25	10675	0.03	973	10960	0.035	995
CSTE	1-3	2.5	0.25	11954	0.023	989	12501	0.023	995

*All dimensions are in inches, all stresses are in psi, and all loads are in lbs.

Table 4-7 Summary of nonlinear properties for each FPT test configuration

2-3 Plane FPT Summary for 2.5" Specimen with Spherical Contact Surfaces			
Non Linear Properties	**Nonlinear**	**LOG**	**AVERAGE**
G	462272	451840	457056
K	36483	31009	33746
N	0.226	0.199	0.213

2-3 Plane FPT Summary for 1" Specimen with Spherical Contact Surfaces			
Non Linear Properties	**Nonlinear**	**LOG**	**AVERAGE**
G	407709	408952	408331
K	27499	30304	28901
N	0.163	0.181	0.172

2-3 Plane FPT Summary for 1" Specimen with Cylindrical Contact Surfaces			
Non Linear Properties	**Nonlinear**	**LOG**	**AVERAGE**
G	341429	353611	347520
K	26386	30841	28614
N	0.162	0.207	0.185

1-3 Plane FPT Summary for 2.5" Specimen with Spherical Contact Surfaces			
Non Linear Properties	**Nonlinear**	**LOG**	**AVERAGE**
G	753702	723088	738395
K	48165	42365	45265
N	0.272	0.233	0.253

1-3 Plane FPT Summary for 1" Specimen with Spherical Contact Surfaces			
Non Linear Properties	**Nonlinear**	**LOG**	**AVERAGE**
G	632007	670636	651322
K	36348	43320	39834
N	0.225	0.280	0.253

1-3 Plane FPT Summary for 1" Specimen with Cylindrical Contact Surfaces			
Non Linear Properties	**Nonlinear**	**LOG**	**AVERAGE**
G	782485	734586	758536

Table 4-7 – Continued

K	42067	44323	43195
N	0.291	0.291	0.291

Chapter 5

Analysis and Discussion

It should be noted that the FPT test method was consistent in the 1-3 plane from standard SBS curves. In addition the linear region of SBS test data in the 2-3 plane was consistent with the linear region produced from FPT in the 2-3 plane. This provides indication that the nonlinear curve in the 2-3 plane is accurately measuring shear strain in the 2-3 plane. However, more research should be conducted to verify coupling does not exist with FPT test method and that the interlaminar shear strains measured are pure shear strain. Sensitivity was noticed between the nonlinear method and the logarithmic linear method when trying to extract the nonlinear properties G, K, and N. This is due to multiple solutions that will satisfy the Ramberg-Osgood equation and still produce the same curve. It should be stated that sensitivity on the convergence of the stress strain curve was conducted to determine the effect of this and was noticed that the converged curve itself was not affected. Although the nonlinear properties varied by 3% - 4% the curve was not affected. The FPT test method proved to be a reliable test method to extract the interlaminar shear stress-strain curve the 2-3 plane at a high enough percent strain to construct the nonlinear curve. The sensitivity of the test to different size specimen and contact surfaces produced similar results and by changing configurations only the peak strain was affected. The FPT test method should be considered reliable to accurately produce the nonlinear interlaminar shear stress strain curve in the 1-3 and 2-3 planes.

The interlaminar shear stress-strain curve is consistent with the each of the FPT tests. The 2.5” specimen produced the highest load of all that tests at 995 lbs. but experienced the lowest strain percent of all the tests at 3% in the 2-3 plane and 2.3% in the 1-3 plane. The 1.0” specimen with the 0.25” cylindrical contacts experienced the

highest strain percent of all the tests at 5.2% in the 2-3 plane and 4.9% in the 1-3 plane. However, the interlaminar shear stress-strain curve in the 2-3 plane shifted downward by 13.2%. Due to the dependency of σ_{22} in the 2-3 plane coupling could exist in the 2-3 plane when cylindrical contact surfaces are used and should be investigated. It was noticed that the contact pressures were limited to the edge of the specimen due to localized bending at the corners of the specimen. Figure 5-1 illustrates how the localized bending at the corners effect the ability for the straight cylindrical to make contact uniformly along the surface of the specimen. This test method was also the most visibly constrictive to capture DIC due to shadows cast from the contact surfaces.

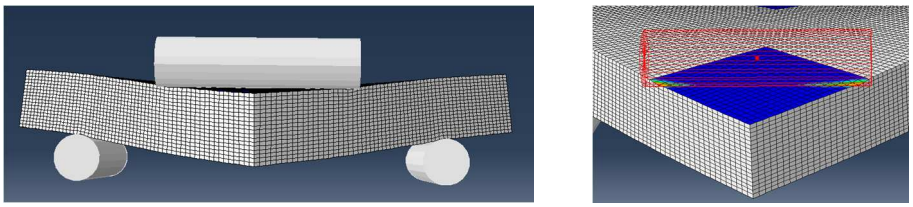

Figure 5-1 Contact pressure from the cylindrical contact surfaces

It was shown that by modifying the specimen dimensions and contact diameters and configurations that the nonlinear interlaminar shear stress strain curve was consistent for each test method. The 1.0” specimen with the 0.25” spherical contact surfaces in the 2-3 plane experienced 4.9% strain in the 2-3 plane and 3.5% strain in the 1-3 plane. Although each test experienced different peak loads, stresses, and strains, the nonlinear curve was consistent. Figure 5-2 shows the final converged interlaminar shear stress-strain curve for each test method in the 2-3 plane and the 1-3 plane is shown in Figure 5-3. The peak strains are indicated at the termination of each of the curves.

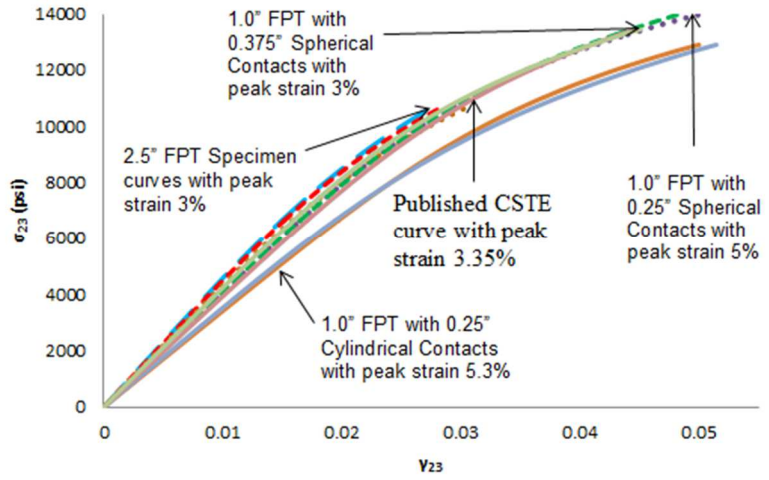

Figure 5-2 Final converged interlaminar shear stress-strain curves for each FPT test in the 2-3 plane

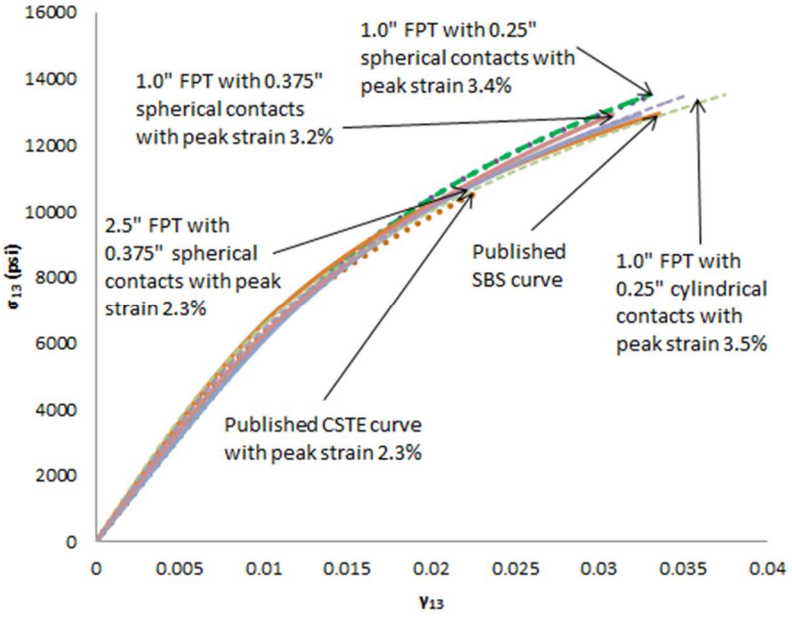

Figure 5-3 Final converged interlaminar shear stress-strain curves for each FPT test in the 1-3 plane

The 1" specimen with 0.25" spherical contact surfaces provided the most consistent shear strain data collected by DIC. This is because they did not cast shadows

on the specimen and limit the ability for DIC to see the complete specimen field of view. The average curve from the 1” specimen in the 1-3 plane and 2-3 plane is shown in Figure 5-4 and is validated in the 1-3 plane with the SBS curve in the 1-3 plane.

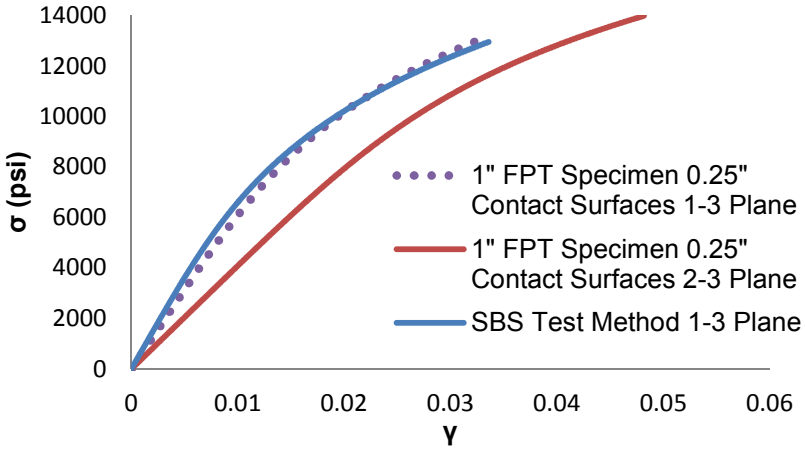

Figure 5-4 1” FTP specimen with spherical contacts in the 2-3 plane and validated in the 1-3 plane with SBS

Chapter 6

Conclusion

The development and implementation of composite structures has grown rapidly through the aerospace industry exceeding our ability to characterize the material properties due to costly and time consuming test methods. To fully understand complex deformation and failure mechanisms in more complex structures, three-dimensional material properties are required. With the use of the digital image correlation (DIC) technique and finite element analysis (FEA), short beam shear (SBS) tests have been modified to include the measurement of multiple material constitutive properties, including nonlinear interlaminar shear stress-strain curves. SBS shear and V-notch testing are limited to measuring linear shear material properties in the 2-3 direction, due to premature tensile failure due to bending before the stress-strain curve becomes nonlinear. By loading a specimen in compression using the flat FPT test method, significant nonlinear shear strain is developed on all principal material planes. Numerous test configurations and parameters were considered to determine the sensitivity of the FPT test method and the ability for it to capture the material properties in the 2-3 plane. Analysis of the 1-3 plane using the FPT method was verified with SBS testing. Analysis in the 2-3 plane is confirmed to SBS testing in the 2-3 plane in the linear region.

Analysis was conducted to produce the nonlinear interlaminar shear stress-strain curve in the 2-3 plane and to determine the sensitivity of different test configurations to verify if pure shear strain is being measured experimentally using DIC. Unidirectional carbon tape IM7 8552 was used in the FPT testing. Different test configurations were analyzed by varying the size of the specimen and contact surfaces and test fixtures in order to determine the sensitivity and reliability of the FPT test method when using it to extract material. FPT specimens were varied by length, width, and

thickness to analyze the nonlinear shear stress strain curve each test method produced. Spherical and cylindrical contact surfaces were both considered in varying dimensions to determine the sensitivity of the placement of the contact surfaces. Using experimental strains determined from DIC as an initial approximation FEA calculated the shear stress in an iterative process and was plotted with the experimental strains from DIC. The results from the different tests provide the interlaminar shear stress-strain curve and the interlaminar shear material properties in principal material planes for the different FPT test configurations. The interlaminar shear stress strain curve in the 1-3 plane was compared using the FPT test method and the SBS test method. Analysis shows a matching trend for these nonlinear curves giving an indication that FPT is measuring pure strain in the 1-3 plane. The interlaminar shear stress strain curve in the 2-3 plane was compared using the FPT test method and the SBS test method in the linear region. SBS can measure shear strain in the 2-3 plane in the linear region and this trend is consistent with the shear stress stain curve produced from the FPT test method. Varying dimensions of small square specimens were considered with varying dimensions of spherical and cylindrical contact surfaces. The curve produced from each test method indicated similar trends but failed at different peak strain values. This indicates that the shear strain measured experimentally was not affected by the change in test setup except in the 2-3 plane with the cylindrical rollers.

Further research should be conducted to validate the FPT test method for different types of composites such as S-Glass and woven composites and to extend it to the 1-2 plane to completely provide all three-dimensional properties simultaneously. Analysis shows the cylindrical contact surfaces are consistent with the other tests however more investigation into the 2-3 plane is needed to understand if coupling occurs using this test method. In order to accurately predict and analyze composites, 3

dimensional properties are needed. This will aid in design analysis to help lower cost, weight, testing, and analysis time by using experimentally calculated results rather than assumptions. Nonlinear interlaminar shear properties in the 2-3 plane cannot be determined experimentally using traditional SBS test methods because the specimen will fail prematurely in tension before the curve become nonlinear. Using the flat plate torsion method along with the digital image correlation technique the nonlinear interlaminar shear stress strain curve can be obtained experimentally.

References

1. **Tsai, SW.** *Experimental determination of the elastic behavior of orthotropic plates.* s.l. : J Eng Ind, 1965. (August): 315-8.

2. **Howell, Robert A.** *An Experimental Investigation of the Bifurcation in Twisted Square Plates.* s.l. : The University of British Columbia, 1991.

3. **Gommers, B, Verpoest, I and Van Houtte, P.** *Further Developments in Testing and Analysis of the Plate Twist Test for In-Plane Shear Modulus Measurements.* Great Britian : Elsevier Science Limited, 1996. Composites Part A 27A.

4. **De Morais, A.B, Cardoso, C.M and Pereira, A.B.** *Evaluation of in-plane ply shear properties from unidirection plate torsion tests.* Santiago : Elsevier Ltd., 2013. Composites Part A 53.

5. *In quest of methods for measuring 3D mechaical properties of composites.* **Makeev, Andrew, et al., et al.** 5826, s.l. : Elsevier Ltd. , 2014, Vol. CSTE.

6. **Daniel, Isaac M and Ishai, Ori.** *Engineering Mechanics of Composite Materials .* Oxford : Oxford University Press, 2006.

7. **Hexcel Corporation.** *HexTow IM7 Carbon Fiber Product Data.* Stamford : Hexcel Corporation, 2013.

8. —. *HexPly 8552 Product Data.* Stamford : Hexcel Corporation, 2013.

9. —. *HexPly Prepreg Technology.* Stamford : Hexcel Corporation, 2013. FGU 017C.

10. **Correlated Solutions.** Correlated Solutions Non-Contact Measuring Solutions. [Online] [Cited: January 23, 2014.] www.correlatedsolutions.com/digital-image-correlation-2.

11. **Dassault Systemes.** *Abaqus Analysis User's Manual Volumn IV.* 2010.

12. **Carpenteir, Paige.** *Advanced Materials Characterization Based on Full Field Deformation Measurements.* Arlington : University of Texas Arlington, 2013.

13. **Logan, Darly L.** *A First Course in Finite Element Method.* Stamford : Global Engineering, 2012.

14. **GreenBerg, Michael D.** *Advanced Engineering Mathematics.* Upper Saddle River : Prentice-Hall, Inc., 1998.

15. **Steif, Paul S.** *Mechanics of Materials .* Upper Saddle River : Pearson Higher Education, Inc. , 2012.

16. **i.imgur.com/g4nvA.jpg.** *USN Northrop Grumman RQ-4 Global Hawk.*

17. **Sun, C.T.** *Mechanics of Aircraft Structures.* Hoboken : John Wiley & Sons, 2006.

18. **Seon, Guillaume.** *Finite Element Based Methodology for Prediction of Matrix-Dominated Failures in Composites.* Arlington, Texas : University of Texas Arlington, May 2014.

Biographical Information

Gary Steven Grohman Jr. was born on June 22, 1983 in Pasadena, Texas. He moved to Corpus Christi, Texas where he graduated from Flour Bluff High School. After high school Steven began a career in the aviation industry as a fuel system repair mechanic for preventative maintenance and AOG situations on numerous aircraft. After 4 years Steven decided to move to Dallas Texas to pursue an education.

Steven transferred jobs to a production assembly line aircraft mechanic at Vought Aircraft in 2005 and enrolled into The University of Texas Arlington for the Bachelor of Science in Aerospace Engineering program. He obtained his Associates of Arts degree for Tarrant County Community College in 2009. In 2010 Steven was selected for an internship at Vought Aircraft and was moved into the testing and research and development lab where he learned to test many different aircraft structures from the coupon level to full scale testing. In May of 2011 Steven graduated with a B.S. Aerospace Engineering and a Minor in Mechanical Engineering from the University of Texas Arlington. He started his Master of Science in Aerospace Engineering in June.

Upon graduation in 2011 Steven became employed at the testing and research center at formally Vought Aircraft, currently Triumph Aerostructures, and was given an opportunity to do testing with Digital Image Correlation. This type of technology was new to the company and quickly grabbed his interest. Steven was introduced to, at the time, a new department at The University of Texas Arlington, The Advanced Materials and Structures Lab under the direction of Dr. Andrew Makeev. In May of 2015 Steven obtained his Masters of Science Degree in Aerospace Engineering.

After graduation Steven plans to continue his career in the aerospace industry and pursue a MBA. He wants to thank everyone who made this journey possible because without the support of everyone these accomplishments would not have been possible.